Damage Quantification Using Mode Converted Guided Wave Based 1D Damage-Spectral Element

M. N. Murthy Patnaik

Structures Group, UR Rao Satellite Center, ISRO, Bangalore, India 560017.

K. Renji

UR Rao Satellite Center, ISRO, Bangalore, India 560017. E-mail: renjikna@gmail.com

K. V. Nagendra Gopal

Dept. of Aerospace Engineering, Indian Institute of Technology, Madras, Chennai, India 600036.

(Received 19 March 2024; accepted 25 July 2024)

Quantifying the sizes of the damages in structures using guided waves is an emerging technology. It needs a suitable mathematical model that represents the behavior of the guided waves as they travel through the structure. Though finite element based theoretical models can provide insight into the behavior, they are computationally very costly. Spectral element is a promising solution in this regard. Quantifying the damage using a mode-converted wave based spectral element has not been reported yet. In this work, a spectral element that represents the characteristics of wave propagation, scattering and mode conversion caused by asymmetric notch-type damage in an isotropic waveguide is presented. This frequency domain damage-spectral element is formulated through a combination of three structural waveguides by enforcing appropriate force equilibrium conditions. The spectral element is able to represent the wave scattering and mode conversion due to the presence of the damage. This spectral element is employed in analyzing the wave propagation in a beam that has damage and the characteristics obtained are in agreement with the results expected based on time-of-flight calculations and those obtained using the finite element method. The relation between the depth of the damage and the magnitude of the mode-converted wave for notch-type damage is established using this spectral element and compared with the experimental result. Usage of the same spectral element in quantifying the length of the damage based on the reflections of the primary propagating wave from the damage ends is also demonstrated.

NOMENCLATURE

A	Area of cross-section
A_o	Fundamental anti-symmetric wave mode
$\mathbf{a}$	Column vector of coefficients for describing the displacement
b	Width of the beam
C_1, C_2, C_3, C_4, C_5, C_6	Coefficients used in describing the displacement
d	Depth of the notch
E	Young's modulus of the material
$\mathbf{F}$	Transverse force, a column vector
$\hat{\mathbf{F}}_e$	Fourier coefficient of element force, a column vector
h	Thickness of the beam
h_1	Offset of beam axis
I	Area moment of inertia of the cross-section
k_r, k_1, k_2	Wavenumbers
$\mathbf{K}$	Dynamic stiffness matrix
L	Length of the beam
L_1, L_2, L_3	Length of beam segments
$\hat{\mathbf{M}}$	Spectral load, moment
N	Total number of FFT points
$\hat{\mathbf{N}}$	Spectral load, axial
S_o	Fundamental symmetric wave mode
t	Time
$\mathbf{T}_1$, $\mathbf{T_2}$	Matrices relating displacement / force to the coefficients C_i
u	Axial displacement
$\dot{u}$	Axial velocity
$\hat{u}$	Fourier coefficient of axial displacement
$\mathbf{U}$	Displacement field, a column vector
$\hat{\mathbf{U}}$	Fourier coefficient of displacement field, a column vector
$\hat{\mathbf{U}}_e$	Fourier coefficient of element displacement, a column vector
v	Transverse displacement
$\dot{v}$	Transverse velocity (m/s)
$\hat{v}$	Fourier coefficient of transverse displacement
$\hat{\mathbf{V}}$	Spectral load, shear
λ	Wavelength
μ	Micro unit
ϕ	Angular displacement
$\hat{\phi}$	Fourier coefficient of rotational displacement
ω_n	Circular frequency
ρ	Density of the material

1. INTRODUCTION

Structural health monitoring (SHM) using techniques that are based on ultrasonic guided waves is promising due to its ability to inspect large structures over long distances with a small number of transducers. One of the commonly observed defects in many structural components is the surface damage like cracks, notches etc. These defects are asymmetrically located along the structural depth direction. When the guided waves interact with these asymmetric discontinuities, a mode conversion occurs.[1–3] Hosseini et al.[4] have proposed a new SHM approach based on the mode conversion phenomenon to detect small damages in cellular plate structure by employing high frequency guided waves. This method uses Time of Flight (ToF) calculation of the converted mode for possible damages. Patnaik et.al.[5] demonstrated the convenience of using a mode-converted wave in locating damage in an aerospace structure. In a recent work,[6] mode-conversion of guided waves in Glass Fiber Reinforced Polymer (GFRP) is used to identify fatigue damage accumulation. Among the various parameters studied, it was observed that the matrix-crack density majorly contributes to the mode-conversion effect and results were found to be remarkably useful in composite fatigue life evaluation. In many occasions, the damage detection is done by comparison with the image obtained without the presence of the damage. Zhang et al.[7] developed an accurate damage detection imaging approach by utilizing the mode-converted wave without needing a baseline image. The Probability-based Diagnostic Imaging (PDI) method is integrated with the Converted Mode Extraction (CME) technique and the Damage Index (DI) is obtained based on the time-domain energy of the converted mode.

In addition to the location of the damage, information on the size of the damage is also essential for any SHM program. When a mode-converted wave is used for detecting the damage, it is advisable to use the features of the converted wave itself for quantifying the damage too. However, studies on the quantification of damage based on the characteristics of the mode-converted wave are seldom reported.[5] This work is an attempt in shedding more light on these types of studies.

To assess the size of the damage, one needs to establish a relation between the magnitude of the mode-converted wave and the size of the damage. The relation should be experimentally proven. Obtaining these relations experimentally for various values of the sizes of the damages is a cumbersome process as a large number of tests needs to be performed. Therefore, a practical approach is to have a mathematical model that represents the mode conversion aspect and then determine the relation through simulations for various values of the size of the damage. A validation of the theoretical curve thus obtained can be done for specific sizes of the damage through experimental results.

Theoretical modeling of damages like surface cracks has been done using analytical and semi-analytical methods. In these works,[8–10] the damage is detected based on the changes in natural frequencies and mode shapes. A similar technique has been applied using FE and mode synthesis for detecting cracks in beams[11,12] and delaminations in composite beams.[13,14] As a noticeable change in the natural frequencies will be seen in higher order modes, a change in the characteristics of the propagation of waves is a more suitable method than change in the natural frequency to detect damage.

Wave propagation in various structural elements like 1-D waveguides (rods, beams), 2-D waveguides as platelike structures has been studied in detail for a considerable period. Various continuum models[15,16] and discrete models[17–19] of wave propagation were developed and employed. Analytical solutions for the scattering of the guided waves due to damage in the structure are difficult to obtain. Numerical methods like the Finite Element method (FEM), Boundary Element Method (BEM) are suitable for solving wave propagation problems. Cho[20] has utilized the hybrid BEM along with the experimental phase velocity concept for capturing the mode-conversion phenomenon in a plate having varying thickness. In this study, it is noted that a waveguide with symmetric variation in thickness causes mode-conversion within the modes of the family whereas, in the case of an asymmetric thickness variation, mode-conversion occurs in a different mode family. Discrete models have the advantage of modeling complex geometries and boundary conditions but suffer from various issues associated with proper spatial discretization required for solving wave propagation problems and are computationally expensive. Studies conducted in literature[21,22] capture the mode conversion phenomena in several delaminated composite beams using 3D FE models and involve significant computational time. Patnaik et al.[5] attempted to quantify the damage using the mode-converted wave. The relation between the magnitude of the wave and the size of the damage is obtained through FEM. Due to the large size of the model, FEM is not a viable solution and hence the above relation is obtained only for a few sizes of the damages. Among many discrete methods employed for modeling the phenomenon of wave propagation in structures, the Spectral Element Method (SEM) is an effective and convenient tool. The frequency based Spectral Finite Element Method (SFEM) was developed by Doyle[19,23] and is widely in use.

Analysis of wave propagation in a cracked rod,[24] a cracked beam[25] and a plate with a crack[26] by SEM was studied in which the crack in the structural members was modeled as a dimensionless spring. The changes in the modal parameters are utilized to identify the presence of a crack and its location. The lacuna with the above method of modeling is that it doesn't represent the wave scattering at the damage edges and mode conversion. It has been reported that in case of large damage, wave reflections would occur from both ends of the damage, which is not represented in these models.[27]

A damage-spectral element with embedded through-width delamination is developed to study the wave propagation in a composite beam[28] and the results are compared with the FEM. However, in this work, the damage quantification is not addressed, and also the mode conversion is not discussed. Hu et al.[29] proposed a cracked spectral element based on SEM and verified its wave propagation and damage features by conventional FEM results. Here the reflection and transmission wave coefficients are used for damage feature extraction and the mode-converted wave is not considered. It is seen that though there are several spectral elements that can represent wave propagation characteristics, spectral elements that ad-

dress the mode conversion phenomena when the wave interacts with the damage are not frequently reported. He and Ng[1] and Carnam et al.[30] present spectral elements formulated in the time domain, that simulate scattering and mode conversion but are not convenient when a large number of computations need to be completed. A frequency based spectral element is more convenient for the analysis and interpretation. As most of the damages encountered in practice are asymmetric and mode conversion of the guided waves occurs when they reach a damage, there is a need to develop a spectral element that represents this behavior and can be employed for damage identification and quantification.

In this work, a frequency domain spectral element that models a notch-type of damage located asymmetrically in the thickness direction of an isotropic beam is presented. The element formulation models the damage zone and the surrounding integral regions as one waveguide. Enforcing the equilibrium at the interface and employing appropriate kinematic boundary conditions reduce to a single element that represents embedded damage. The results of the damage-spectral element are validated by FEM simulations. The damage-spectral element is then used in quantifying the depth and length of the damage. The relation between the amplitude of the mode-converted wave and the depth of the damage is presented for a typical isotropic beam and compared with experimental results.

2. 1D DAMAGE-SPECTRAL ELEMENT

SEM has been established as a powerful tool for analyzing the propagation of waves in structures. SEM combines the high accuracy of the conventional spectral methods with the advantages of the FEM.[16,23] The spectral element approach is based on the global approximation of analyzed functions using basis functions and then with precision solving the differential equation. As a result, the analysis can be computed with a few elements without losing accuracy.

In the frequency-based SEM, the governing differential equations are first transformed from the time domain to the frequency domain using Discrete Fourier Transform (DFT). Fast Fourier Transform (FFT) is used for computational implementation. This transformation changes the Partial Differential Equations (PDEs) into a set of Ordinary Differential Equations (ODEs) having frequency as a variable. The spatial variation is obtained by solving the characteristic equation in k-space (wavenumber space). This results in a complex dynamic shape function matrix as a linear superposition of all the wave modes. Following the conventional FE method, the global dynamic stiffness matrix is formed which is exact. The global system is solved for the spectral amplitude of the applied load history at each frequency. By performing inverse FFT, the time domain response is obtained.

2.1. Beam Spectral Element

Consider a rectangular beam of length L, thickness h and width b, as shown in Fig. 1. The displacement field at a point has three components, namely the longitudinal displacement $u(x,t)$, the transverse displacement $v(x,t)$ and the rotation of the cross-section of the beam $\varphi(x,t)$ which are all functions

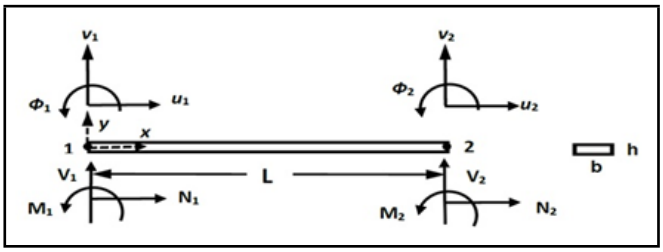

Figure 1. Beam element with coordinate system and degrees of freedom.

of x and time. The displacement field can be represented by a column vector $\mathbf{U}(x,t)$ as:

$$\mathbf{U}(x,t) = \{u(x,t), v(x,t), \varphi(x,t)\}^T. \tag{1}$$

Using Fourier Transform, the displacement $u(x,t)$, can be written as:

$$u(x,t) = \sum_{1}^{N} \hat{u}(x,\omega_n) e^{i\omega_n t}; \tag{2}$$

where ω_n is the circular frequency and N is the number of points taken for FFT. Function $\hat{u}(x,\omega_n)$ is the Fourier coefficient at frequency ω_n for the displacement at x.

Similarly, other displacements can also be defined and the Fourier components in the column vector form is:

$$\hat{\mathbf{U}}(x,\omega_n) = \{\hat{u}(x,\omega_n), \hat{v}(x,\omega_n), \hat{\varphi}(x,\omega_n)\}^T. \tag{3}$$

The displacement field can now be represented by the column vector:

$$\mathbf{U}(x,t) = \sum_{1}^{N} \hat{\mathbf{U}}(x,\omega_n) e^{i\omega_n t}. \tag{4}$$

The Fourier coefficients will be of the form:[20]

$$\hat{u}(x) = C_1 e^{-ik_r x} + C_4 e^{-ik_r (L-x)}; \tag{5}$$

$$\hat{v}(x) = C_2 e^{-ik_1 x} + C_3 e^{-ik_2 x} + C_5 e^{-ik_1 (L-x)} + C_6 e^{-ik_2 (L-x)}; \tag{6}$$

$$\hat{\varphi}(x) = \frac{\partial \hat{v}(x)}{\partial x}; \tag{7}$$

where C_1, C_2, C_3, C_4, C_5, and C_6 are determined from the boundary conditions.

Substituting the expressions for the field variables given by Eq. (4) in the governing differential equation of a beam with an axial load,[20] the wavenumbers k_r, k_1 and k_2 can be obtained as:

$$k_r = \omega_n \sqrt{\frac{\rho}{E}}; \tag{8}$$

$$k_1 = \pm\sqrt{\omega_n} \left(\frac{\rho A}{EI}\right)^{1/4}; \quad k_2 = \pm i\sqrt{\omega_n} \left(\frac{\rho A}{EI}\right)^{1/4}; \tag{9}$$

where E denotes Young's modulus and ρ the density of the material. Cross-section of the beam has an area of A and its second moment of area is I. The imaginary unit is represented by $i = \sqrt{-1}$.

With known wavenumbers at a particular frequency ω_n, the generalized displacements at the nodes of the 1-D element

(having nodes-1 and 2) can be expressed in the form

$$\begin{Bmatrix} \hat{u}(0,\omega_n) \\ \hat{v}(0,\omega_n) \\ \hat{\varphi}(0,\omega_n) \\ \hat{u}(L,\omega_n) \\ \hat{v}(L,\omega_n) \\ \hat{\varphi}(L,\omega_n) \end{Bmatrix} = \hat{\mathbf{U}}_e = [\mathbf{T}_1]\{\mathbf{a}\}. \tag{10}$$

Elements of $[\mathbf{T}_1]$ are as per Eqs. (5) to (7), evaluated at the given frequency. It is a 6×6 non-symmetric and non-singular matrix. As $[\mathbf{T}_1]$ is a matrix with several expressions,[20] it is not reproduced here for brevity. The column vector $\{\mathbf{a}\}$ is the unknown coefficient vector at the same frequency, given as:

$$\{\mathbf{a}\} = \{C_1, C_2, C_3, C_4, C_5, C_6\}^T. \tag{11}$$

The nodal spectral loads for the element, $\hat{\mathbf{N}}\rightarrow$ axial,$\hat{\mathbf{V}}\rightarrow$ shear and $\hat{\mathbf{M}}\rightarrow$ bending moment can be determined by differentiating the spectral displacement with respect to x. Using appropriate relationships, they can be expressed as:

$$\begin{Bmatrix} \hat{N}_1 \\ \hat{V}_1 \\ \hat{M}_1 \\ \hat{N}_2 \\ \hat{V}_2 \\ \hat{M}_2 \end{Bmatrix} = \hat{\mathbf{F}}_e = [\mathbf{T}_2]\{\mathbf{a}\}. \tag{12}$$

The matrix $[\mathbf{T}_2]$ has similar properties as those of $[\mathbf{T}_1]$.

Finally, the nodal forces and nodal displacements can be related and the dynamic stiffness matrix of the beam spectral element can be written as

$$\hat{\mathbf{F}}_e = [\mathbf{T}_2][\mathbf{T}_1]^{-1}\hat{\mathbf{U}}_e = [\mathbf{K}_e]\hat{\mathbf{U}}_e. \tag{13}$$

The matrix $[\mathbf{K}_e]$ is the spectral element dynamic stiffness matrix, which is of size 6×6.

SFEM provides a methodology to make the wave propagation analysis suitable for incorporation in the framework of the FEM[23,31] and facilitates the global matrix assembly. The displacement field variables are derived at various frequency points and the time domain response is obtained by using an inverse DFT. A single node semi-infinite spectral element can be incorporated by choosing $L = \infty$ in Eqs. (5) and (6). Reflection at the fixed boundary can be represented by assigning a large value for E.[23,32]

2.2. Spectral Element for Embedded Damage

The spectral element representing the characteristics of the waves traveling across a damage is referred to here as the damage-spectral element. It has two nodes, namely node-1 and node-2. The element covers the damage and the region on both sides of the damage.

For developing the damage-spectral element, the beam is subdivided into three regions, namely the damage region of length L_3 and two integral regions of length L_1 and L_2 of thickness h on either side of the damage region as shown in Fig. 2. The depth of the notch is d. Each region is modeled as a beam spectral element as described in Section 2.1 to arrive at the damage-spectral element.

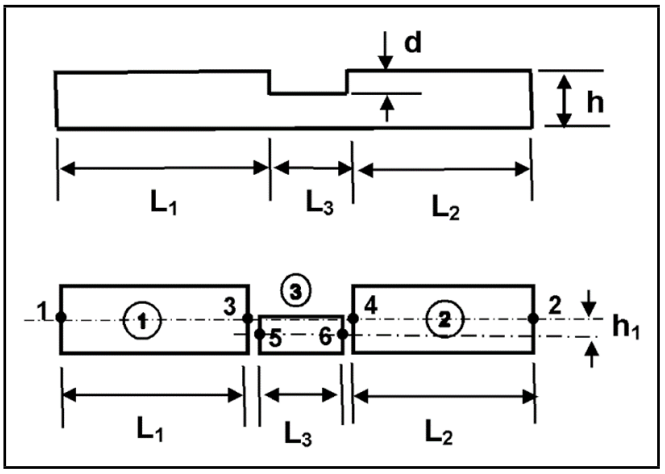

Figure 2. Beam with notch: the damage zone modeled by 1-D beam waveguides.

The notch zone of the beam is represented by element-3, whose axis is offset from the beam axis by h_1. The length of this element is equal to the notch length L_3. Portions of the beam adjacent to the notch are modeled as element-1 and element-2 of length L_1 and L_2 respectively. The formulation is such that the nodes 3, 4, 5 and 6 will be internally eliminated and only nodes 1 and 2 will be remaining. It is to be noted that whether damage is present or not, there will be only one element connecting the nodes 1 and 2. In the absence of damage, a beam spectral element will connect the nodes whereas the damage-spectral element developed in this work can be used to connect the nodes, if there is damage.

Using the dynamic stiffness matrix for the beam as given by Eq. (13) and applied to j^{th} element of the damage-spectral element ($j = 1, 2, 3$) gives:

$$[\mathbf{K}_j]\hat{\mathbf{U}}_j = \hat{\mathbf{F}}_j. \tag{14}$$

For convenience, the dynamic stiffness matrix which is 6×6 is partitioned into 4 matrices, each of size 3×3. The displacement vector and the force vector are partitioned into two matrices of size 3×1, the top one representing the displacements and forces at the first node and the bottom one representing the same at the second node. Thus, for the j^{th} element with p and q representing the first and the second node, the set of equations becomes:

$$\begin{bmatrix} \mathbf{K}^j_{11} & \mathbf{K}^j_{12} \\ \mathbf{K}^j_{21} & \mathbf{K}^j_{22} \end{bmatrix} \begin{Bmatrix} \hat{\mathbf{U}}_p \\ \hat{\mathbf{U}}_q \end{Bmatrix} = \begin{Bmatrix} \hat{\mathbf{F}}_p \\ \hat{\mathbf{F}}_q \end{Bmatrix}. \tag{15}$$

For the first element p and q are 1 and 3, for the second element p and q are 4 and 2, and for the third element p and q are 5 and 6. At this stage, there are 18 (6 for each element) displacement variables.

Transverse displacement and slope at node-5 are the same as those at node-3 and similarly at node-6 and node-4. This leads

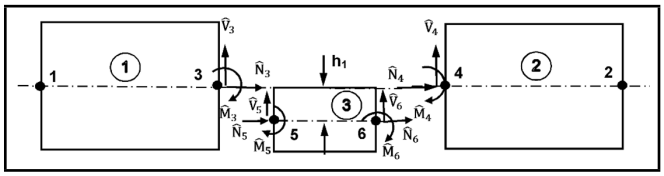

Figure 3. Force balance at the interface of the damage.

to the following conditions:

$$\hat{\mathbf{U}}_5 = \begin{Bmatrix} \hat{u}_5 \\ \hat{v}_5 \\ \hat{\varphi}_5 \end{Bmatrix} = \begin{Bmatrix} \hat{u}_3 - h_1\phi_3 \\ \hat{v}_3 \\ \hat{\varphi}_3 \end{Bmatrix} = \mathbf{S}_1\hat{\mathbf{U}}_3; \tag{16}$$

$$\hat{\mathbf{U}}_6 = \begin{Bmatrix} \hat{u}_6 \\ \hat{v}_6 \\ \hat{\varphi}_6 \end{Bmatrix} = \begin{Bmatrix} \hat{u}_5 - h_1\phi_5 \\ \hat{v}_5 \\ \hat{\varphi}_5 \end{Bmatrix} = \mathbf{S}_1\hat{\mathbf{U}}_4; \tag{17}$$

$$\text{where } \mathbf{S}_1 = \begin{bmatrix} 1 & 0 & -h_1 \\ 0 & 1 & 0 \\ 0 & 0 & 1 \end{bmatrix}. \tag{18}$$

Force balance at the left side of the notch, shown in Fig. 3, gives the following relations:

$$\begin{Bmatrix} \hat{N}_3 \\ \hat{V}_3 \\ \hat{M}_3 \end{Bmatrix} + \begin{Bmatrix} \hat{N}_5 \\ \hat{V}_5 \\ \hat{M}_5 \end{Bmatrix} + \begin{Bmatrix} 0 \\ 0 \\ -h_1\hat{N}_5 \end{Bmatrix} = \begin{Bmatrix} 0 \\ 0 \\ 0 \end{Bmatrix}. \tag{19}$$

This can be expressed in the matrix form as

$$\hat{\mathbf{F}}_3 + \mathbf{S}_1^T\hat{\mathbf{F}}_5 = 0. \tag{20}$$

Similar force balance at the right side of the notch leads to

$$\hat{\mathbf{F}}_4 + \mathbf{S}_1^T\hat{\mathbf{F}}_6 = 0. \tag{21}$$

Consider spectral element-3 and applying the relations as per Eq. (15)

$$\begin{bmatrix} \mathbf{K}_{11}^3 & \mathbf{K}_{12}^3 \\ \mathbf{K}_{21}^3 & \mathbf{K}_{22}^3 \end{bmatrix} \begin{Bmatrix} \hat{\mathbf{U}}_5 \\ \hat{\mathbf{U}}_6 \end{Bmatrix} = \begin{Bmatrix} \hat{\mathbf{F}}_5 \\ \hat{\mathbf{F}}_6 \end{Bmatrix}. \tag{22}$$

Pre-multiplying on both sides of Eq. (22) by $\mathbf{S}_1^T$ and expressing $\hat{\mathbf{U}}_5$ and $\hat{\mathbf{U}}_6$ in terms of $\hat{\mathbf{U}}_3$ and $\hat{\mathbf{U}}_4$:

$$\begin{bmatrix} \mathbf{S}_1^T\mathbf{K}_{11}^3\mathbf{S}_1 & \mathbf{S}_1^T\mathbf{K}_{12}^3\mathbf{S}_1 \\ \mathbf{S}_1^T\mathbf{K}_{21}^3\mathbf{S}_1 & \mathbf{S}_1^T\mathbf{K}_{22}^3\mathbf{S}_1 \end{bmatrix} \begin{Bmatrix} \hat{\mathbf{U}}_5 \\ \hat{\mathbf{U}}_6 \end{Bmatrix} = \begin{Bmatrix} \mathbf{S}_1^T\hat{\mathbf{F}}_5 \\ \mathbf{S}_1^T\hat{\mathbf{F}}_6 \end{Bmatrix}. \tag{23}$$

The forces $\hat{\mathbf{F}}_5$ and $\hat{\mathbf{F}}_6$ are related to $\hat{\mathbf{F}}_3$ and $\hat{\mathbf{F}}_4$ as per Eq. (20) and Eq. (21) and hence Eq. (23) can be expressed as:

$$\begin{bmatrix} \mathbf{S}_1^T\mathbf{K}_{11}^3\mathbf{S}_1 & \mathbf{S}_1^T\mathbf{K}_{12}^3\mathbf{S}_1 \\ \mathbf{S}_1^T\mathbf{K}_{21}^3\mathbf{S}_1 & \mathbf{S}_1^T\mathbf{K}_{22}^3\mathbf{S}_1 \end{bmatrix} \begin{Bmatrix} \hat{\mathbf{U}}_5 \\ \hat{\mathbf{U}}_6 \end{Bmatrix} = \begin{Bmatrix} -\hat{\mathbf{F}}_3 \\ -\hat{\mathbf{F}}_4 \end{Bmatrix}. \tag{24}$$

Writing the governing equations for element-1 and 2 in the form of Eq. (15) and those of element-3 in the form of Eq. (24) and then assembling them leads to the set of equations in the form:

$$\begin{bmatrix} \mathbf{K}_{11}^1 & \mathbf{K}_{12}^1 & 0 & 0 \\ \mathbf{K}_{21}^1 & \mathbf{K}_{22}^1+\mathbf{S}_1^T\mathbf{K}_{11}^3\mathbf{S}_1 & \mathbf{S}_1^T\mathbf{K}_{12}^3\mathbf{S}_1 & 0 \\ 0 & \mathbf{S}_1^T\mathbf{K}_{21}^3\mathbf{S}_1 & \mathbf{K}_{11}^2+\mathbf{S}_1^T\mathbf{K}_{22}^3\mathbf{S}_1 & \mathbf{K}_{21}^2 \\ 0 & 0 & \mathbf{K}_{21}^2 & \mathbf{K}_{22}^2 \end{bmatrix} \begin{Bmatrix} \hat{\mathbf{U}}_1 \\ \hat{\mathbf{U}}_3 \\ \hat{\mathbf{U}}_4 \\ \hat{\mathbf{U}}_2 \end{Bmatrix} = \begin{Bmatrix} \hat{\mathbf{F}}_1 \\ \mathbf{0} \\ \mathbf{0} \\ \hat{\mathbf{F}}_2 \end{Bmatrix}. \tag{25}$$

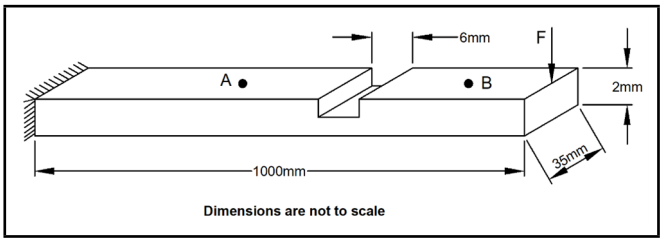

Figure 4. Schematic of the beam with notch.

While forming the above, $\hat{\mathbf{F}}_3$ and $\hat{\mathbf{F}}_4$ vanish as there are no external forces at these nodes.

Eliminating the internal degrees of freedom of $\hat{\mathbf{U}}_3$ and $\hat{\mathbf{U}}_4$ by static condensation,[33] we get:

$$[\overline{\mathbf{K}}]_{6\times6} \begin{Bmatrix} \hat{\mathbf{U}}_1 \\ \hat{\mathbf{U}}_2 \end{Bmatrix} = \begin{Bmatrix} \hat{\mathbf{F}}_1 \\ \hat{\mathbf{F}}_2 \end{Bmatrix}; \tag{26}$$

where $[\overline{\mathbf{K}}]$ is the stiffness matrix for the damage-spectral element.

This damage-spectral element can be implemented in MATLAB® and can be incorporated at the damage zone along with the normal beam elements. Results of the wave propagation analysis done using this element are given subsequently.

The spectral elements reported so far are for delamination in composite laminates and not for surface defects like notch. Also, the work reported[27,28] do not address the mode conversion. The damage-spectral element presented here models surface defects and represents the mode conversion of the primary propagating wave. The developed element is later applied for quantifying the depth and length of the damage.

3. WAVE PROPAGATION IN BEAM HAVING DAMAGE

Wave scattering and mode conversion generated by damage in an isotropic beam are analyzed using the developed damage-spectral element to verify its performance. The element formulation is implemented in MATLAB® and numerical simulations are carried out. The results obtained using the spectral element are compared with the expected results which are based on ToF and validated by FEM.

3.1. Details of the Beam

A cantilevered beam of length 1 m and having a through-width notch-type damage, as shown in Fig. 4, is considered. The width of the beam is 35 mm and the thickness is 2 mm. The damage is in the form of a through-width notch having a length of 6 mm and depth of 1 mm, as shown in Fig. 4. The damage is located at a distance of 700 mm from the fixed end of the beam. A transverse force $\mathbf{F}$ which is a modulated sine pulse of five cycles at a frequency of 120 kHz and amplitude of 1 N, as shown in Fig. 5, is applied at the free end of the beam.

The response at $\mathbf{A}$ and $\mathbf{B}$ located at a distance of 400 mm and 865 mm respectively from the fixed end are studied for wave scattering and mode conversion caused by the damage. These locations are on either side of the damage. Location $\mathbf{B}$ is at a distance of 165 mm and location $\mathbf{A}$ is at a distance of 300 mm from the damage.

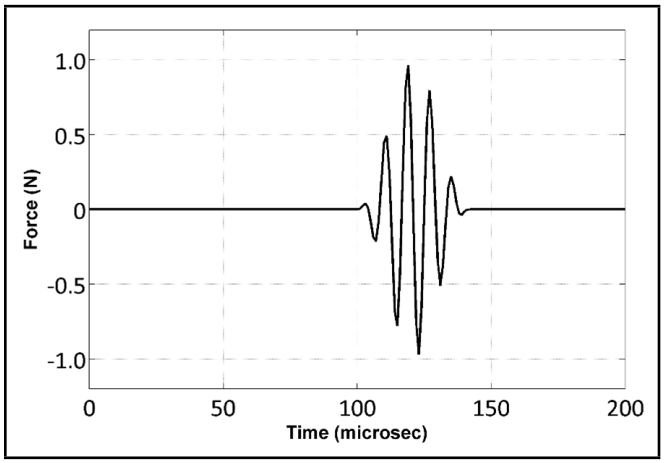

Figure 5. Excitation pulse at 120 kHz.

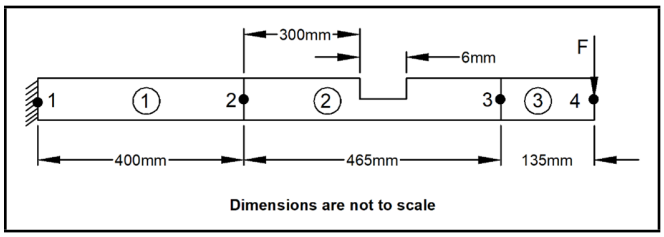

Figure 6. Spectral finite element model of the beam with notch.

3.2. Spectral Element Model

Ideally, the entire beam can be modeled by a single damage-spectral element to capture the wave propagation and scattering due to the damage. However, to obtain responses at specific nodes, the beam is discretized into three elements as shown in Fig. 6, where element-2 is the damage-spectral element developed in this work. To simulate the fixed conditions at one end, a throw-off element having a high value of Young's modulus of elasticity is assumed. A transverse force pulse, as shown in Fig. 5 is applied at node-4 and the velocity response at nodes-2 and 3 (corresponding to points **A** and **B** on the beam) are analyzed. Results are obtained for cases of the beam without damage and with the presence of the damage.

3.3. Results Using Spectral Element

The transverse velocity response ($\dot{v}$) at node-3 of the beam having the damage is shown in Fig. 7, superimposed on the response of the beam without having the damage. Since the excitation of the beam is by a transverse force, fundamental anti-symmetric wave (A_0 mode) is generated, which is the incident wave pulse-1. In the case of the beam without the damage, the velocity response shows the incident fundamental anti-symmetric, A_o wave (pulse-1) and the A_0 wave reflected from the beam fixed end (pulse-7), whereas the response of the beam having the damage has several additional reflected wave pulses from the damage as well as the free end of the beam (pulse: 2-6).

The paths of the waves traveling along the beam are schematically shown in Fig. 8. The length of the notch is 6 mm but for clarity of visualization the notch is shown larger and it is not to scale. As the propagating wave frequency is 120 kHz, there is only one wave pulse reflecting from the other end of the damage and hence the waves from the two ends of the crack

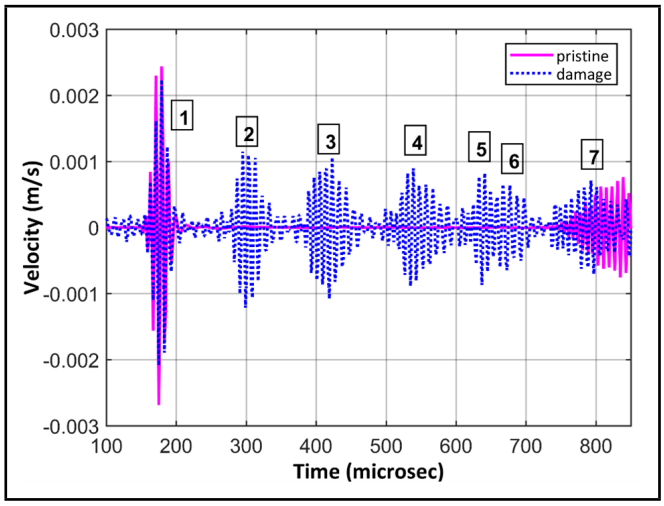

Figure 7. Transverse velocity response at node-3.

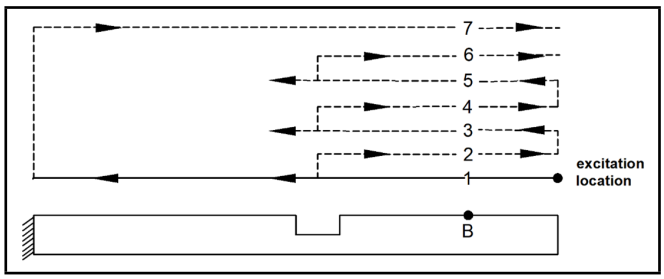

Figure 8. Schematic of path of wave pulse reaching node-3 (point **B**).

are not distinguishable. To avoid several waves being shown, reflection from the damage is indicated to be at the center of the damage which is only for representation. The group velocity of A_o mode at 120 kHz generated in the beam is calculated as 2950 m/s and that of S_o is 5000 m/s.

Consider the results at node-3 of the pristine beam. It is to be noted that the pulse is initiated at 100 μs. As per the results using the spectral element, the pulse arrives at node-3 at 143 μs. Based on the speed of the wave and the distance of node-3 from the point of excitation, the A_o wave is expected to reach node-3 at 146 μs. The A_o wave travels past node-3 and it is expected to arrive back at node-3 after a reflection at the fixed end. Considering the speed of this wave and the distance traveled by this wave, the pulse is expected at 585 μs after the first pulse which is at 731 μs. The response computed using the spectral element shows the arrival of this pulse at 738 μs. The results show that the spectral element correctly represents the wave transmission in the pristine beam.

Let us now consider the results of the beam having the damage. Pulse-1 is the incident A_0 wave pulse and pulse-7 is the A_0 wave that reflected from the fixed end. The wave pulses-2,4 and 6 are expected to be the first, second and third reflections of A_o from the damage, whereas pulses-3 and 5 are the waves reflected (same as incident A_o and not newly generated) from the free end of the beam. As node-3 is at a distance of 165 mm from the damage, it is expected that the pulse-2 will arrive at 258 μs and pulse-3 at 349 μs and so on. It can be seen from the results shown in Fig. 7 that the damage-spectral element developed here represents accurately the wave transmission in a beam having damage.

One important characteristic of wave propagation around

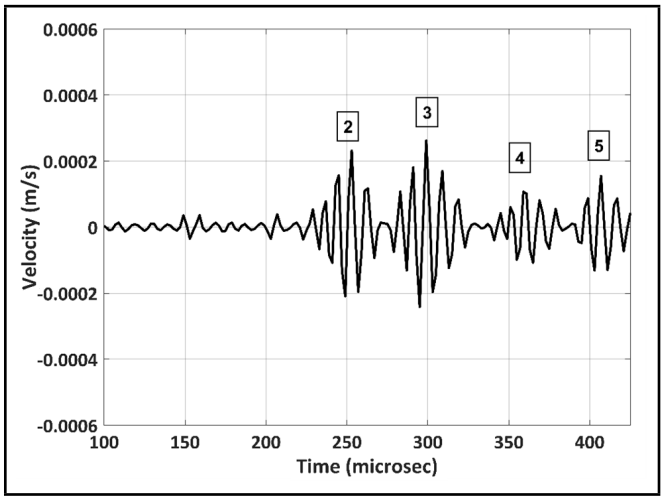

Figure 9. Axial velocity response at node-3.

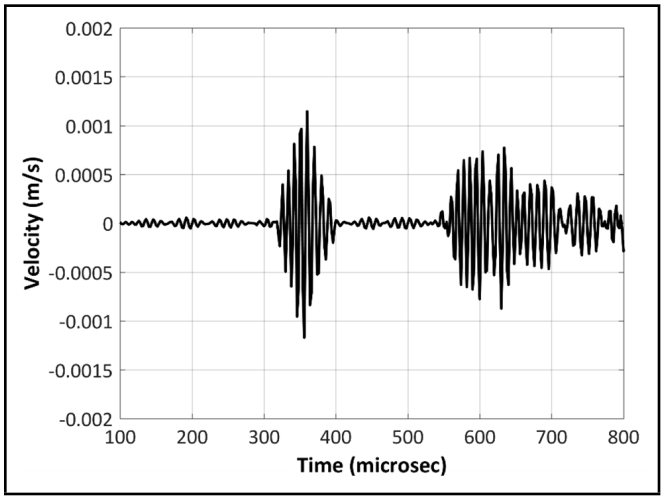

Figure 10. Transverse velocity response at node-2.

an asymmetrically located damage is the mode conversion.[1–3] The A_o mode upon interaction with the notch-type damage generates So mode, which also propagates in the beam. Owing to the difference in their group velocities, the mode-converted So mode is distinct and doesn't interact with the A_o mode. As it is a longitudinal mode, its presence can be well revealed by the axial velocity response. The axial velocity ($\dot{u}$) at node-3 computed using the spectral element is shown in Fig. 9. The incident wave will not be seen as it has no axial component. The first wave pulse corresponds to the mode-converted S_o wave that originated from the damage and traveled to node-3. Further wave pulses seen are their reflections from the free end of the beam and the reflections from the damage as could be expected from Fig. 8. As it is a S_o wave, the first pulse in Fig. 9 (marked as 2 in the figure) should arrive at 235 µs and the second pulse at 289 µs. The results obtained using the spectral element, shown in Fig. 9, are in very good agreement with the ToF calculations. Thus, it can be seen that the developed damage-spectral element represents the mode conversion caused by asymmetrically located damage.

The transverse and axial velocities at node-2 (point A) are also computed, shown in Figs. 10 and 11, respectively. In the transverse velocity response, the first pulse arriving at node-2 should be the incident A_o wave and hence it should appear at

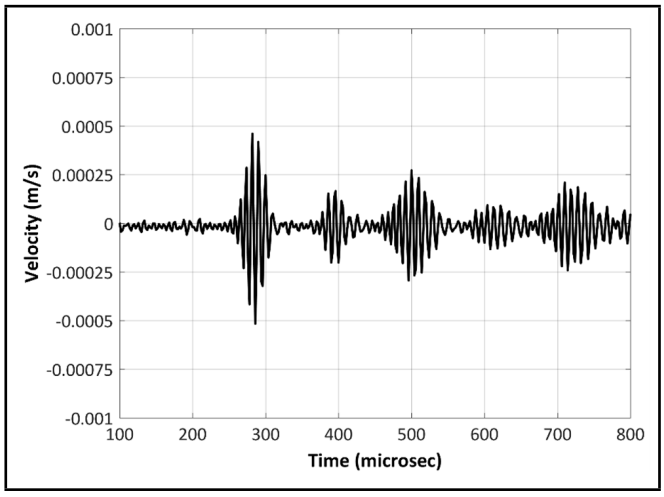

Figure 11. Axial velocity response at node-2.

304 µs. The response estimated using the spectral element is in agreement with this. The second pulse is that reflected from the fixed end.

For the axial velocity response, as the mode-converted S_o wave generated at the damage has a higher group velocity, it reaches node-2 at 262 µs which is prior to the arrival of propagating A_o mode. This behavior is clearly shown by the axial velocity response estimated using the developed spectral element, shown in Fig. 11.

Thus, it is noted that the spectral element developed in this work represents the wave propagation characteristics in a beam having surface damage. It represents the mode conversion of the guided wave which is caused due to the damage.

4. VALIDATION BY FEM

It is shown in Section-3 that the developed spectral element represents the mode conversion caused by asymmetrical damage and its correctness was verified through the time-of-flight calculations. Here, the responses obtained from the damaged spectral element are compared with the conventional FEM results and subsequently, the damage-spectral element is used for damage quantification.

The beam described in Section 3.1 is modeled in conventional FEM using 1D-beam elements consisting of 4000 elements. The size of the element is selected such that to have a fine mesh to model the notch length of 6 mm and to accurately capture the amplitude of the mode-converted wave. The length of the element is about 0.25 mm. A point load is applied at the free end node of the cantilever in the form of the pulse as shown in Fig. 5 and transient response analysis is carried out. The FE model of the beam idealized with element offset is shown in Fig. 12. A zoomed-in view of the notch zone can also be seen in Fig. 12. The responses are obtained at locations **A** and **B**. The locations are shown in Fig. 4. It is noted that the beam of 1 m length is represented by three elements in the SEM model whereas the FEM model has around 4000 elements.

Figure 13 shows the transverse velocity response at location **A** obtained from FEM and compared with the corresponding response using the damage-spectral element. This shows a good match at a location beyond the damage along the wave

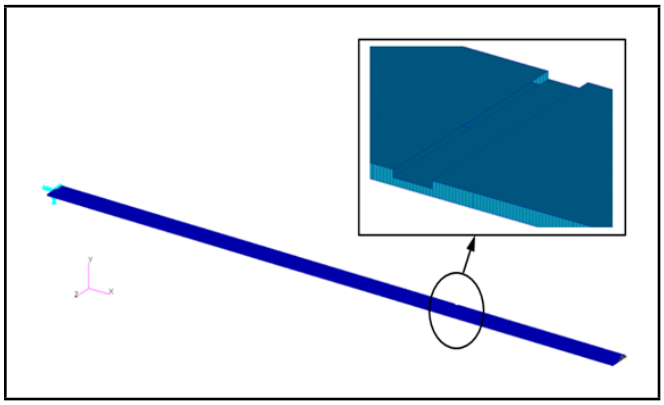

Figure 12. FE model of the beam.

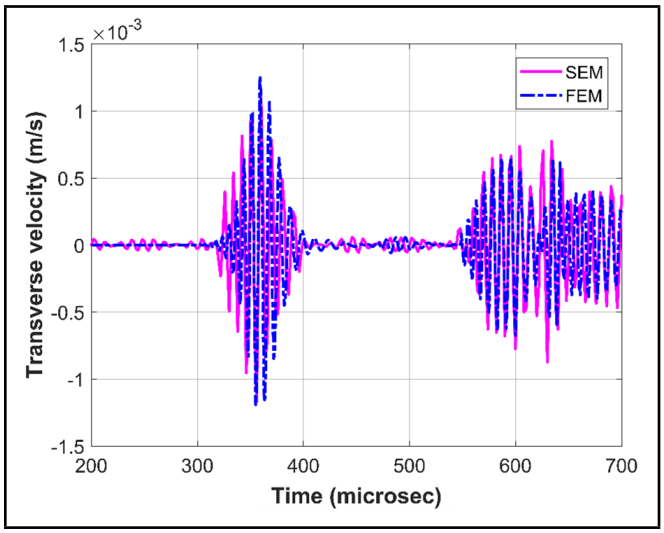

Figure 13. Transverse velocity at location **A** using damage-spectral element and FEM.

transmission path and validates the formulation of the damage-spectral element. As this spectral element is to represent the mode conversion, the most important response to be verified is the axial response, shown in Fig. 14 for location **B** (node-3 of SEM).

The instances of arrival time of the S_o wave and its amplitudes match very well, proving the ability of the damage-spectral element to capture the wave scattering due to the damage. The results have some differences between 100 μs and 220 μs. As FFT and inverse FFT are involved, the time domain response by SEM shows computational noise. However, this is less than 8 percent of the peak amplitude of the mode-converted wave. The situation can be improved by considering a slightly higher number of FFT points.

5. DAMAGE QUANTIFICATION USING SEM

The amplitude of the mode-converted wave is influenced by the size of the damage. If the relation between them can be established, the quantification of the damage in the given structure can be inferred from the measured amplitude of the mode-converted wave. The relations between the amplitude of the mode-converted guided wave and the size of the notch have been now obtained using the damage-spectral element.

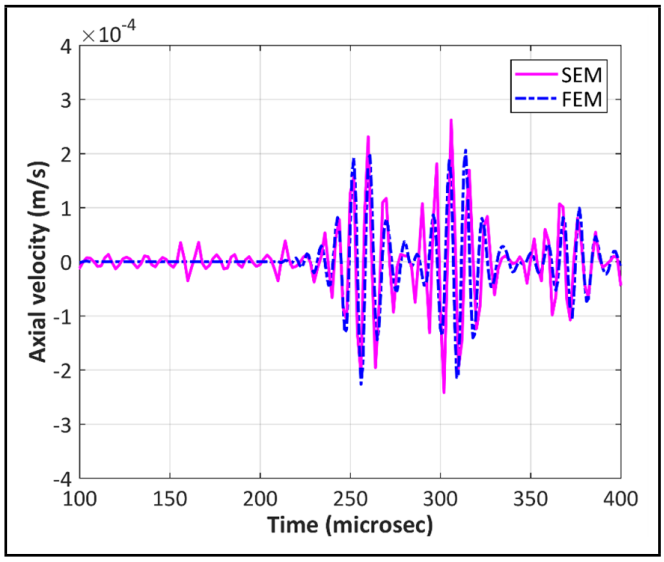

Figure 14. Axial velocity at location **B** using damage-spectral element and FEM.

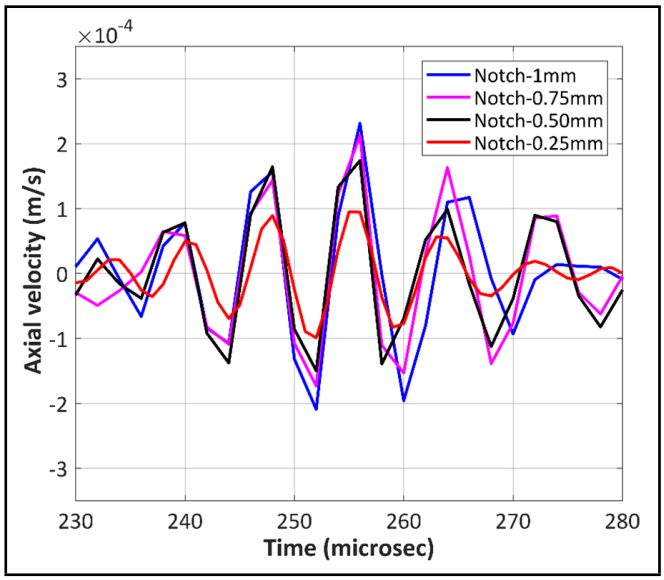

Figure 15. Axial velocity response for varying notch depth.

5.1. Quantification of Notch Depth

Simulations are carried out for various notch depths by varying the values of h_1. A transverse force pulse as shown in Fig. 5 is applied at the free end node-4 of the beam. The axial velocity responses at node-3 are computed and given in Fig. 15. The wave pulse seen is the mode-converted S_o wave generated at the damage and its magnitude increases with an increase in damage size. It can be seen that they are very distinct for various values of depth.

Variation of the peak magnitude of the mode-converted wave for various values of the depth of the notch is now plotted using the developed damage-spectral element and it is shown in Fig. 16. The normalization is done with respect to the magnitude of the mode-converted wave when the notch depth is 1 mm, that is for a depth of half of the thickness. These plots can be used for arriving at the depth of the notch from the known magnitude of the mode-converted S_o pulse.

It is good to have verification with the results obtained using other techniques. The experiments were conducted[5] for notch

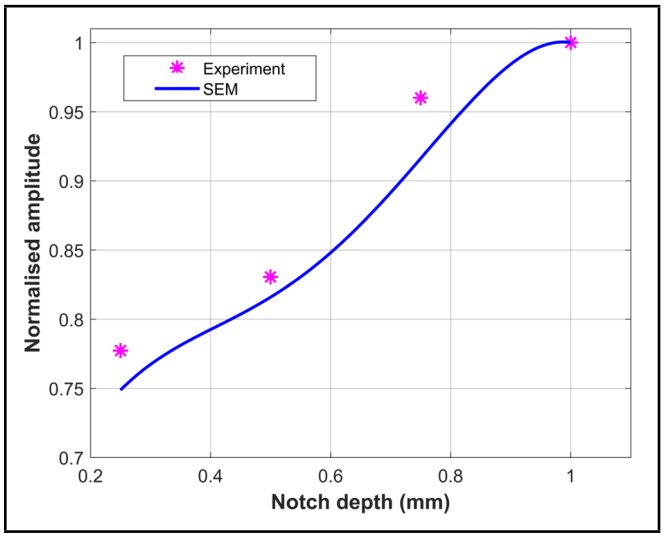

Figure 16. Variation of peak magnitude of the mode-converted wave velocity with notch depth.

sizes of 0.25 mm, 0.5 mm, 0.75 mm and 1 mm. The experimental setup, measurements and the procedures of conducting the experiments are as given in an earlier work[5] and hence not repeated here. Experimentally obtained values are also shown in Fig. 16. It can be seen that the results obtained using the spectral element are in good agreement with those obtained through experiments. The magnitude of the mode-converted wave in the experiment is consistently slightly higher compared to those obtained using the spectral element.

In an earlier work, Patnaik et al.[5] had used commercial FE software ABAQUS v6.12 for the above purpose. The system run time taken for one simulation, that is for one value of the notch, was several hours whereas it has taken a few seconds while using this spectral element. Therefore, generating the curve given in Fig. 16 through FEM has not been tried here. It needs to be noted that by using this spectral element the time taken for computation is extremely low and does not need to have costly commercial software.

In summary, the results show that the developed damage-spectral element is capable of capturing the changes in wave characteristics due to the presence of damage. It allows one to study the differences in the wave transmission characteristics for various parameters of the damage using a computationally efficient spectral element without needing any commercial software and utilize them for the assessment of the size of the damage. The methodology is demonstrated for a typical case and one can apply it to the specific application.

5.2. Quantification of Notch Length

Determining the length of the damage from the mode-converted wave is very complex. However, it can be quantified from the ToF of the reflections of the primary propagating wave from the ends of the notch. It requires that the wavelength (λ) of the propagating wave be comparable to the size of the damage.[1,27] The damage-spectral element presented in this work can be used to perform this, which is demonstrated here.

A beam having a notch as shown in Fig. 17 is modeled using the damage-spectral element. For this purpose, the primary propagating wave that gets reflected at the damage (A_o mode)

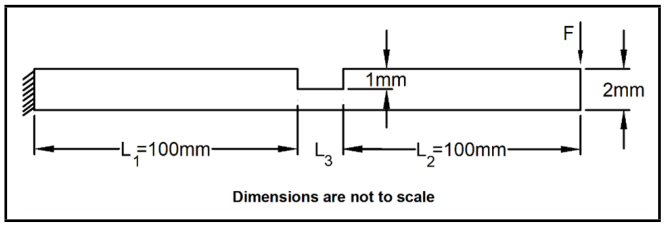

Figure 17. Dimensional parameters of beam with damage.

is used. A transverse force of modulated five cycle pulse of 1 N magnitude at 500 kHz is applied at the free end of the beam. Simulations are carried out for various values of the notch length 'L3' and the transverse velocity response at the tip of the beam is captured. The beam tip response is considered for the study to get distinct wave reflections from the damage ends and without interaction with the reflected waves from the fixed end. The notch lengths studied are 5 mm, 10 mm, 20 mm and 30 mm which approximately represent $\lambda/2$, λ, 2λ and 3λ of the propagating A_o mode at 500 kHz.

Figure 18 shows the transverse velocity response of the beam for different notch lengths. It is noticed that when the length of the damage is less than the wavelength of the propagating A_o wave, the reflection from the right and the left ends of the damage get merged onto a single wave packet as seen in Fig. 18(a). As the length of the damage increases beyond the wavelength as seen in Fig. 18(b) to (d), the wave packets reflected from the damage appear from each end of the damage. Distinct waves are clearly seen for damages having lengths greater than λ. It is also observed that the amplitude of the wave reflected from the farthest end of the damage is larger. The length of the damage estimated based on the difference in ToF of the reflected waves from the ends of the damage in Fig. 18(c) is 18.4 mm which is close to the actual notch length of 20 mm. Similarly, the estimated length of the damage from Fig. 18(d) is 28.5 mm against the actual value of 30 mm. Hence the damage-spectral element presented in this work can be very well used for characterizing the length of the damage.

Thus, it is demonstrated that the damage-spectral element presented in this work can very well be used to quantify the depth and length of the damage. The depth of the notch is identified using the mode-converted wave and the length of the damage is identified through the reflected primary propagating mode when excited using an anti-symmetric guided wave.

6. CONCLUSIONS

A frequency domain damage-spectral element to represent a notch-type of damage in a beam located asymmetrically across the section was presented. The developed damage-spectral element was able to represent the wave scattering and mode conversion generated by a non-symmetric type of damage. The results obtained using this spectral element were very much in agreement with those obtained through FEM simulations. The notch-type damage was characterized by its depth and length and can be modeled by a single spectral element. This damage-spectral element can be employed in quantifying the depth and length of the damage. The spectral element was able to precisely capture the variation of response of the mode-converted wave with a change in depth of the damage. The magnitude

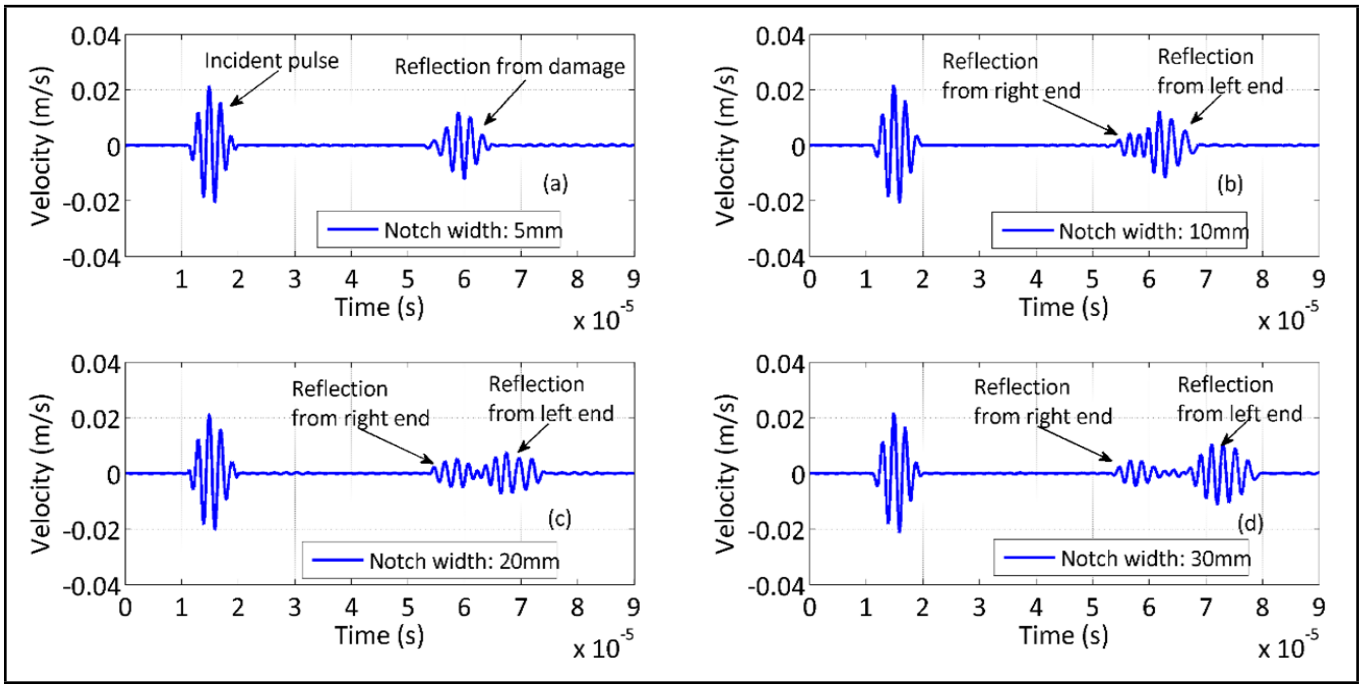

Figure 18. Transverse velocity response at the beam end for varying notch length.

of the mode-converted wave increased with the depth of the notch. A typical relation between the amplitude of the mode-converted wave and the depth of the notch in an isotropic beam was presented. The curve was in agreement with the experimental results. The damage length was quantified based on the ToF variation in the reflected waves from the ends of the damage, provided the wavelength of the propagating wave was comparable with the size of the damage. The amplitude of the wave reflected from the farthest end of the damage was larger. The spectral element was capable of capturing both the depth and length of the notch. The time needed for computation was extremely low and also there was no need to use any commercial FEM software. The inherent computational advantage of spectral finite element analysis coupled with the use of damage-spectral element will be very efficient for SHM applications.

REFERENCES

[1] He, S. and Ng, C. T. Analysis of mode conversion and scattering of guided waves at cracks in isotropic beams using time-domain Spectral Finite Element Method, Special issue: Structural Health Monitoring, *Electronic Journal of Structural Engineering*, **14** (1), 20–32, (2015). https://doi.org/10.56748/ejse.141861

[2] Ramadas, C., Krishnan Balasubramaniam, Joshi, M., and Krishnamurthy, C. V. Interaction of guided Lamb waves with an asymmetrically located delamination in a laminated composite plate, *Smart Materials and Structures*, **19** (6), 065009, (2010). https://doi.org/10.1088/0964-1726/19/6/065009

[3] Benmeddour, F., Grondel, S., Assad, J., and Moulin, E. Study of the fundamental Lamb modes interaction with asymmetrical discontinuities, *Nondestructive Testing & Evaluation International*, **41** (5), 330–340, (2008). https://doi.org/10.1016/j.ndteint.2008.01.004

[4] Hosseini, S. M. H., Duczek, S., and Gabbert, U. Damage localization in plates using mode conversion characteristics of ultrasonic guided waves, *Journal of Nondestructive Evaluation*, **33**, 152–165, (2014). https://doi.org/10.1007/s10921-013-0211-y

[5] Murthy Patnaik, M. N., Renji, K. and Nagendra Gopal, K. V. Detection and quantification of asymmetrically located structural damages by mode converted guided wave using piezo electric elements, *International Journal of Acoustics and Vibration*, **28** (1), 76–85, (2023). https://doi.org/10.20855/ijav.2023.28.11920

[6] Zhang, C., Zhang, Z., Ji, H., Qiu, J., and Tao, C. Mode conversion behavior of guided wave in glass fiber reinforced polymer with fatigue damage accumulation, *Composites Science and Technology*, **192**, 108073, (2020). https://doi.org/10.1016/j.compscitech.2020.108073

[7] Jiaqi, Z., Xu, H., Zhou, K., Yang, Z., Liu, K., Zheng, Y., Ma, S., and Wu, Z. Baseline-free damage diagnostic imaging approach relying on the extraction of converted modes of ultrasonic guided waves, *Journal of Aerospace Engineering*, **34** (6), (2021). https://doi.org/10.1061/(asce)as.1943-5525.0001319

[8] Rizos, P. and Asprgathos, N. Identification of crack location and magnitude in a cantilever beam from the vibrating mode, *Journal of Sound and Vibration*, **138** (3), 381–388, (1990). https://doi.org/10.1016/0022-460x(90)90593-o

[9] Ostachowicz, W. and Krawczuk, M. Analysis of the effect of cracks on natural frequencies of a cantilever beam, *Journal of Sound and Vibration*, **150** (2), 191–201, (1991). https://doi.org/10.1016/0022-460x(91)90615-q

[10] Nandwana, B. and Maiti, S. K. Detection of location and size of crack in stepped cantilever beams based on measurements of natural frequencies, *Journal of Sound and Vibration*, **203** (3), 435–446, (1997). https://doi.org/10.1006/jsvi.1996.0856

[11] Kisa, M. Free vibration analysis of a cantilever composite beam with multiple cracks, *Composite Science and Technology*, **64** (9), 1391–1402, (2004). https://doi.org/10.1016/j.compscitech.2003.11.002

[12] Nahvi, H. and Jabbari, M. Crack detection in beams using experimental modal data and Finite Element Mode, *International Journal of Mechanical Sciences*, **47** (10), 1477–1497, (2005). https://doi.org/10.1016/j.ijmecsci.2005.06.008

[13] Majumdar, P. M. and Suryanarayan, S. Flexural vibrations of beams with delaminations, *Journal of Sound and Vibration*, **125** (3), 441–461, (1985). https://doi.org/10.1016/0022-460x(88)90253-2

[14] Liu, J., Zhu, W., Charalambides, P. G., Shao, Y., Xu, Y., Wu, K., and Xiao, H. Four-beam model for vibration analysis of a cantilever beam with an embedded horizontal crack, *Chinese Journal of Mechanical Engineering*, **29** (1), 163–179, (2016). https://doi.org/10.3901/cjme.2015.0901.108

[15] Rose, J. L. *Ultrasonic Guided Waves in Solid Media*, Cambridge University Press, Cambridge, (2014). https://doi.org/10.1017/CBO9781107273610

[16] Gopalakrishnan, S. *Wave Propagation in Materials and Structures*, CRC Press, Boca Raton, (2016). https://doi.org/10.1201/9781315372099

[17] Zhao, X. and Rose, J. Boundary Element Method for defect characterization potential in a wave guide, *International Journal of Solids and Structures*, **40**, 2645–2658, (2003). https://doi.org/10.1016/s0020-7683(03)00097-0

[18] Ham, S. and Bath, K.-J. A Finite Element Method enriched for wave propagation problems, *Computers and Structures*, **94–95**, 1–12, (2012). https://doi.org/10.1016/j.compstruc.2012.01.001

[19] Doyle, J. F. Determining the location and size of a transverse crack in a beam, *Experimental Mechanics*, **35** (3), 272–280, (1995). https://doi.org/10.1007/bf02319668

[20] Cho, Y. Estimation of ultrasonic guided wave mode conversion in a plate with thickness variation, *IEEE Transactions on Ultrasonics, Ferroelectrics, and Frequency Control*, **47** (3), 591–603, (2000). https://doi.org/10.1109/58.842046

[21] Soleimanpor, R. and Ng, C.-T. Mode conversion and scattering analysis of guided waves at delaminations in laminated composite beams, *Structural Monitoring and Maintenance*, **2** (3), 213–216, (2015). https://doi.org/10.12989/smm.2015.2.3.213

[22] Pudipeddi, G. T., Ng, C.-T., and Kotousov, A. Mode conversion and scattering of Lamb waves at delaminations in composite laminates, *Journal of Aerospace Engineering*, **32** (5), 04019067, (2019). https://doi.org/10.1061/(asce)as.1943-5525.0001060

[23] Doyle, J. F. *Wave Propagation in Structures*, Springer-Verlag, London, (1997).

[24] Palacz, M. and Krawczuk, M. Analysis of longitudinal wave propagation in a cracked rod by the Spectral Element Method, *Composites and Structures*, **80** (24), 1809–1816, (2007). https://doi.org/10.1016/s0045-7949(02)00219-5

[25] Krawczuk, M., Palacz, M., and Ostachowicz, W. The dynamic analysis of a cracked Timoshenko beam by the Spectral Element Method, *Journal of Sound and Vibration*, **264** (5), 1139–1153, (2003). https://doi.org/10.1016/s0022-460x(02)01387-1

[26] Krawczuk, M., Palacz, M., and Ostachowicz, W. Wave propagation in plate structures for crack detection, *Finite Elements in Analysis and Design*, **40** (9–10), 991–1004, (2004). https://doi.org/10.1016/j.finel.2003.03.001

[27] Peng, H., Ye, L., Meng, G., Mustapha, S., and Li, F. Concise analysis of wave propagation using the Spectral Element Method and identification of delamination in CF/EP composite beams, *Smart Materials and Structures*, **19** (8), 85018, (2010). https://doi.org/10.1088/0964-1726/19/8/085018

[28] Nag, A., Roy Mahapatra, D., Gopalakrishnan, S., and Sankar, T. S. A Spectral Finite Element with embedded delamination for modeling of wave scattering in composite beams, *Composites Science and Technology*, **63** (15), 2187–2200, (2003). https://doi.org/10.1016/s0266-3538(03)00176-3

[29] Sun, H., Zhang, A., Qing, X., and Wang, Y. Spectral element method for modeling Lamb wave interaction with open and closed crack, *Journal of Vibroengineering*, **19** (7), 4965–4976, (2017). https://doi.org/10.21595/jve.2017.18284

[30] Yeung, C. and Ng, C. T. Time-domain spectral finite element method for analysis of torsional guided waves scattering and mode conversion by cracks in pipes, *Mechanical Systems and Signal Processing*, **128**, 305–317, (2019). https://doi.org/10.1016/j.ymssp.2019.04.013

[31] Gopalakrishnan, S., Chakraborty, A., and Roy Mahapatra, D. *Spectral Finite Element Method: Wave Propagation, Diagnostics and Control in Anisotropic and Inhomogeneous Structures*, Springer, London, (2008).

[32] Roy Mahapatra, D. and Gopalakrishnan, S. A Spectral Finite Element Model for analysis of axial-flexural-shear coupled wave propagation in laminated composite beams, *Composite Structures*, **59** (1), 67–88, (2003). https://doi.org/10.1016/s0263-8223(02)00228-3

[33] Cook, R. D., Malkus, D. S., Plesha, M. E., and Witt, R. J. *Concepts and Applications of Finite Element Method*, John Wiley & Sons, Inc., New York, (2007).